Quark-Gluon Plasma: from lattice simulations to experimental results

G. Aarts, C. Allton
Department of Physics, College of Science, Swansea University, Swansea, United Kingdom

A. Kelly, J.-I. Skullerud
Department of Mathematical Physics, National University of Ireland Maynooth, Maynooth, County Kildare, Ireland

S. Kim
Department of Physics, Sejong University, Seoul 143-747, Korea

T. Harris, S. M. Ryan
School of Mathematics, Trinity College, Dublin 2, Ireland

M. P. Lombardo
INFN-Laboratori Nazionali di Frascati, I-00044, Frascati (RM) Italy

Abstract. Theoretical studies of quarkonia can elucidate some of the important properties of the quark–gluon plasma, the state of matter realised when the temperature exceeds $\mathcal{O}(150)$ MeV, currently probed by heavy-ion collisions experiments at BNL and the LHC. We report on our results of lattice studies of bottomonia for temperatures in the range $100\,\mathrm{MeV} \lesssim T \lesssim 450\,\mathrm{MeV}$, introducing and discussing the methodologies we have applied. Of particular interest is the analysis of the spectral functions, where Bayesian methods borrowed and adapted from nuclear and condensed matter physics have proven very successful.

1. The plasma of quarks and gluons

Heavy ions colliding at ultrarelativistic energies produce a tiny fireball of a plasma of quarks and gluons — the state of matter thought to have existed slightly after the Big Bang. This experimental program started at the SPS in the 1980s, continued at RHIC and it is now running at the LHC, where the

experiments ALICE, ATLAS and CMS are collecting and analyzing data from the collisions of lead nuclei. The most recent runs reached temperatures of about 500 MeV — approximately 5×10^{12} K — well above the temperature of the crossover from ordinary matter to the plasma of quarks and gluons, estimated to be at about 155 MeV [1, 2].

The analysis of the transition from ordinary matter to the quark-gluon plasma, and the nature of the plasma itself — the spectral properties and the residual interactions — is a very active field of theoretical research [3]. We are concerned with temperatures well above those where the synthesis of the lightest nuclei takes place, so strong interactions alone suffice to describe the system. Hence, the appropriate microscopic description is the relativistic field theory of the strong interactions, Quantum Chromodynamics, QCD. We also know that α_s, the QCD coupling at the scale of the temperatures of interest, can be as large as 0.5 and even larger, so that perturbation theory, which will ultimately be valid for very high temperatures, does not work, at least quantitatively, in the region which we wish to explore here. We therefore need a non-perturbative method, and we choose numerical simulations of QCD discretized on a lattice.

This note is devoted to the presentation of lattice results obtained by the FASTSUM collaboration, in particular those appearing in Refs. [4–7]. It updates and expands previous reviews [8, 9].

1.1. Why bottomonium?

Why is bottomonium such an interesting probe of the medium? We will be concerned with phenomena occurring at, or above, the crossover to a chirally symmetric, deconfined phase. In general both chiral symmetry restoration and deconfinement affect the spectrum of the theory: chiral symmetry will be seen in the light sector, by the degeneracy of the chiral partners. The heavier quarks, however, will be blind to chiral symmetry: $m_u, m_d \ll m_s \simeq T_c \simeq \Lambda_{QCD} \ll m_c, m_b$. For instance only about 15% of the strange mass is due to the breaking of chiral symmetry, and for charm and bottom this contribution is completely negligible — modifications of the spectrum of charmonia and bottomonia come entirely from the gauge dynamics. In very short summary, then, quarkonia are ideal probes of the gluodynamics. Since their size is small, however, the sensitivity to deconfinement is not immediate: the short-range component of the potential, which is responsible for their binding, and hence the fundamental bound states, might well survive in the plasma, while the excited states dissolve. We talk of sequential suppression of quarkonia, and the goal of our studies is to make quantitative these very qualitative considerations.

Charmonia — which are easier to produce experimentally — have been studied since early SPS days. We know by now [10] that the experimental results for charmonia are also sensitive to cold nuclear matter effects which reduce the primordial charmonium number significantly — for instance by about 60% at SPS. There are also competing temporal scales — thermalization of the plasma and formation time of the bound states, as well as the intriguing observation that charmonia production rates at SPS and RHIC are quite similar. The latter effect can be at least in part explained by taking into account a regeneration

mechanism for charmonia (feed-down): the higher dissociation rate at RHIC is compensated by a richer feed-down. All these considerations make the study of charmonium suppression patterns extremely fascinating but also challenging.

Bottomonium production, on the other hand, is much less prone to regeneration effects, and as such is a more promising observable for the spectral analysis of the quark–gluon plasma [10]. Since bottomonium production requires the larger energies available at the LHC, such data have become available only very recently. In the last few years, results showing sequential Upsilon suppression in PbPb collision at LHC energies have appeared [11, 12], and we will comment on those at the end.

2. Lattice QCD, relativistic and non–relativistic

Lattice calculations are performed in a discretized Euclidean space-time, which introduces technical scales: the lattice spacing a and the lattice spatial size, L. Each characteristic physical scale l should obviously fulfil the constraint $a \ll l \ll L$. Accommodating quarks with vastly different masses then poses a computational challenge.

Our strategy is to treat as accurately as possible the light quarks: in all our studies gauge configurations with dynamical light Wilson-type quark flavours are produced on highly anisotropic lattices. Details of the lattice action and parameters can be found in Refs. [13,14]. For the b quarks we use non-relativistic QCD (NRQCD). In our work we use a mean-field improved action with tree-level coefficients, which includes terms up to and including $\mathcal{O}(v^4)$, where v is the typical velocity of a bottom quark in bottomonium,$v_b^2 \simeq 0.1$. There is no (rest) mass term in the NRQCD action so one can dispense with the demanding constraint $a \ll 1/m_b$. In general, NRQCD relies on the separation of scales between the bottom quark and any other physical scale of the theory: in our work we study temperatures up to $2T_c \simeq 400$ MeV, hence $m_b \gg T$ and the application of NRQCD is fully justified.

3. Correlators in the plasma

In our studies we considered the S wave states Υ and η_b and the P wave states χ_{b0}, χ_{b1}, χ_{b2} and h_b. We found that the correlators in the different P wave channels behave in a very similar way, hence from now on for the P wave states we present results for the χ_{b1} channel only. The gauge configurations are generated with a dynamical first generation of quarks. More recently the strange quark has been added as well [15]: the general features of the results are unchanged, and a systematic, detailed analysis of the effect of a dynamical strange quark is in progress.

There is a further important simplification in NRQCD: to compute propagators we only need to solve an initial value problem, in contrast to the relativistic case where the same computation requires the inversion of a large sparse matrix. In the hadronic phase we expect that the large Euclidean time behaviour of the propagators is dominated by an exponential decay. In the QGP phase, one can use as guidance the behaviour found for free quarks in

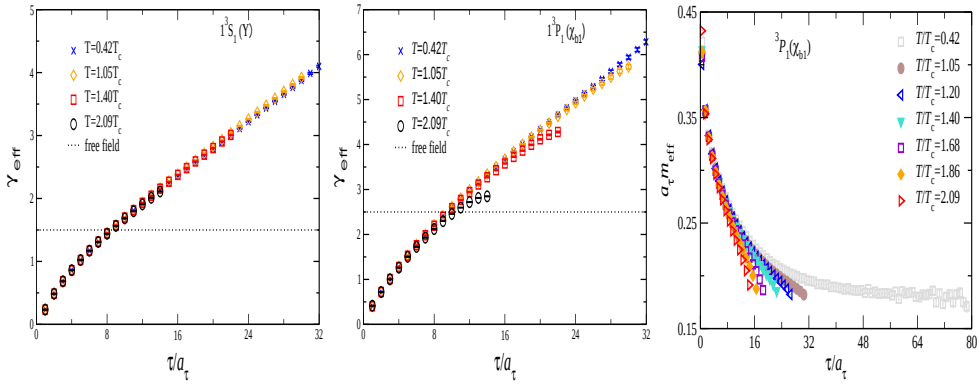

Figure 1. Effective exponents $\gamma_{\rm eff}(\tau)$ for the Υ (left) and χ_{b1} (center), as a function of Euclidean time for various temperatures. The dotted line indicates the non-interacting result in the continuum, which is approached by the χ_{b1} results at the higher temperature $T = 2.1T_c$ [4]. Effective mass for the χ_{b1} (right), as a function of Euclidean time for various temperatures [5].

NRQCD [4, 5, 16], which yields the spectral functions

$$\rho_{\rm free}(\omega) \propto (\omega - \omega_0)^\alpha \, \Theta(\omega - \omega_0), \quad \text{where} \quad \alpha = \begin{cases} 1/2, & \text{S wave.} \\ 3/2, & \text{P wave.} \end{cases} \tag{1}$$

Here we supplemented [15] the free results by a threshold, ω_0, to account for the additive shift in the quarkonium energies which describes the residual interactions in the thermal medium. The correlation functions then have the following behaviour

$$G_{\rm free}(\tau) \propto \int d\omega \, e^{-\omega\tau} \rho(\omega) \propto \frac{e^{-\omega_0 \tau}}{\tau^{\alpha+1}}. \tag{2}$$

To visualize the temperature dependence and at the same time monitor the approach to a quasi-free behaviour we construct effective power plots [4], using the definition

$$\gamma_{\rm eff}(\tau) = -\tau \frac{G'(\tau)}{G(\tau)} = -\tau \frac{G(\tau + a_\tau) - G(\tau - a_\tau)}{2 a_\tau G(\tau)}, \tag{3}$$

where the prime denotes the (discretized) derivative. For a pure power law decay this yields a constant, $\gamma_{\rm eff}(\tau) = \alpha + 1$. Taking into account the threshold ω_0, one finds $\gamma_{\rm eff}(\tau) = \alpha + 1 + \omega_0 \tau$. The results are shown in Fig. 1. We see that the Υ displays a very mild temperature dependence, while for the χ_{b1} the asymptotic behaviour of the effective power tends to flatten out with increasing temperature: this indicates that ω_0 — the slope — decreases with temperature. In the same panel also shown are the effective exponents in the continuum non-interacting limit ($\omega_0 = 0$). In the case of the χ_{b1}, we observe that the effective exponent — which can be read off the intercept of the asympotic straight line

with the $\tau = 0$ axis — seems to approach the non-interacting result. Note that, even for $T \to \infty$ where $\omega_0 = 0$, the effective exponents on the lattice only become a straight line, $\gamma_{\rm eff}(\tau) \to \alpha + 1$, at large enough τ due to the presence of lattice discretisation effects at smaller temporal separations.

A complementary description is offered by the effective masses,

$$a_\tau m_{\rm eff}(\tau) = -\log[G(\tau)/G(\tau - a_\tau)], \tag{4}$$

which are shown in the rightmost panel of Fig. 1. When the correlator takes the form of a sum of exponentials, the ground state will show up as a plateau at large Euclidean times, provided that it is well separated from the excited states. This is indeed the case at the lowest temperature and leads to the zero-temperature spectrum discussed in Refs. [4, 5]. Above T_c, we observe that the effective masses no longer follow the trend given by the correlator below T_c, but instead bend away from the low-temperature data. The results shown in Fig. 1 imply that the spectrum of the χ_{b1} has changed drastically. If isolated bound states persist, the ground state has to be much lighter and excited states cannot be well separated. A more natural explanation is that there is no exponential decay and bound states have melted, immediately above T_c. This interpretation is supported by the spectral function analysis presented next.

4. Spectral functions

Spectral functions play an important role in understanding how elementary excitations are modified in a thermal medium, from many-body physics — see the talk by Giuseppina Orlandini at this meeting [17] — to QCD, which is discussed here.

In general, the spectral decomposition of a (relativistic) zero-momentum Euclidean propagator $G(\tau)$ at finite temperature T is given by

$$G(\tau) = \int_{-\infty}^{\infty} \frac{d\omega}{2\pi} K(\tau, \omega)\rho(\omega), \tag{5}$$

where $\rho(\omega)$ is the spectral function and the kernel K is given by

$$K(\tau, \omega) = \frac{\cosh\left[\omega(\tau - 1/2T)\right]}{\sinh\left(\omega/2T\right)}. \tag{6}$$

In NRQCD the kinematical temperature dependence is always absent. This can be seen in a number of ways. Following Ref. [16], we write $\omega = 2M + \omega'$ and drop terms that are exponentially suppressed when $M \gg T$. The spectral relation (5) then reduces to its zero-temperature limit,

$$G(\tau) = \int_{-2M}^{\infty} \frac{d\omega'}{2\pi} \exp(-\omega'\tau)\rho(\omega'), \tag{7}$$

even at nonzero temperature. Since the interesting physics takes place around the two-quark threshold, $\omega \sim 2M$, the region of interest is around $\omega' \sim 0$ and the lower limit becomes irrelevant. In summary, in the heavy-quark limit the

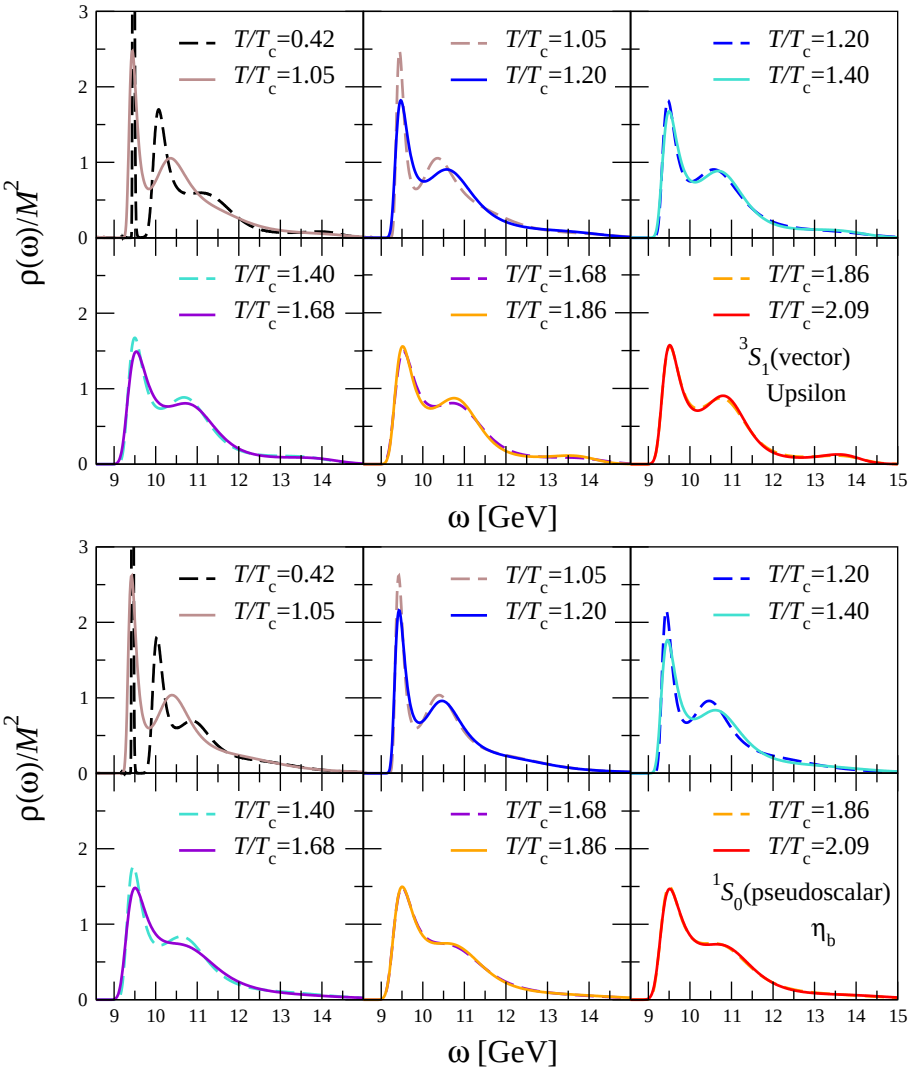

Figure 2. Spectral functions $\rho(\omega)$, normalised with the heavy quark mass, in the vector (Υ) channel (upper panel) and in the pseudoscalar (η_b) channel (lower panel) for all temperature available. The subpanels are ordered from cold (top left) to hot (bottom right). Every subpanel contains two adjacent temperatures to facilitate the comparison [5].

spectral relation simplifies considerably, and temperature effects seen in the correlators are thus only due to changes in the light-quark–gluon system.

Despite these simplifications, the calculation of the NRQCD spectral functions using Euclidean propagators as an input remains a difficult, ill-defined problem. We will tackle it by using the Maximum Entropy Method (MEM) [18], which has proven successful in a variety of applications. We have carefully studied the systematics, including the dependence on the set

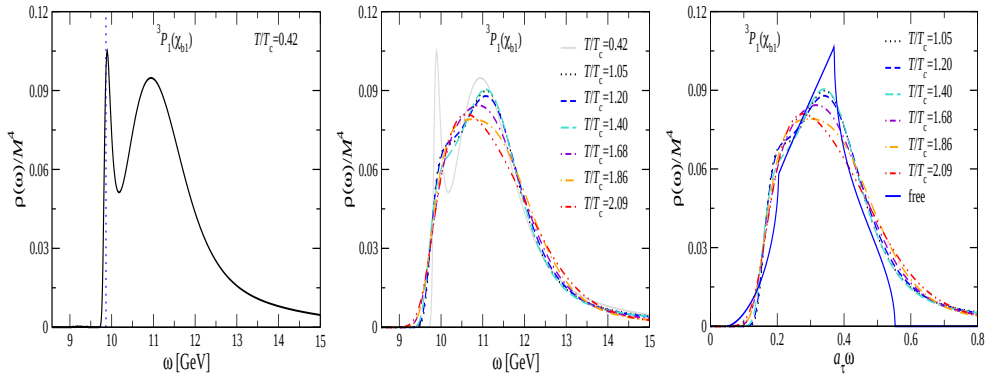

Figure 3. Spectral function in the χ_{b1} channel at the lowest temperature (left) and at all temperatures (center). The dotted line on the left indicates the position of the ground state obtained with a standard exponential fit. Comparison with the free lattice spectral function above T_c (right) [7].

of lattice data points in time, and on the default model $m(\omega)$ which enters in the parametrisation of the spectral function,

$$\rho(\omega) = m(\omega) \exp \sum_k c_k u_k(\omega), \tag{8}$$

where $u_k(\omega)$ are basis functions fixed by the kernel $K(\tau, \omega)$ and the number of time slices, while the coefficients c_k are to be determined by the MEM analysis [18]. We find that the results are insensitive to the choice of default model, provided that it is a smooth function of ω. It remains of interest, and it is an open avenue of research, to experiment with alternative prescriptions [19,20], also on ensembles generated with different lattice actions [21].

The results for the spectral functions for the S wave states, Υ and η_b [5] can be seen in Fig. 2, which shows that as the temperature is increased the ground state peaks of both states remain visible. One caveat applies also here: the apparent width at zero temperature is most likely due to a lattice/MEM artefact, and this calls for an analysis of the discretization effects on the spectral function, which is one of our ongoing projects [22]. The peaks associated with the excited states become suppressed at higher temperature and are no longer discernible quickly above T_c.

Turning now to the P wave states, the result at the lowest temperature is given in Fig. 3 (left). The dotted vertical line indicates the mass of the lowest-energy state obtained with an exponential fit. We see from this that the narrow peak in the spectral function corresponds to the ground state. The second, wider structure is presumably a combination of excited states and lattice artefacts, see below. We note that we have not been able to extract the mass of the first excited state with an exponential fitting procedure. The spectral functions for all temperatures are shown in Fig. 3 (center). We find no evidence of a ground state peak for any of the temperatures above T_c. This is consistent

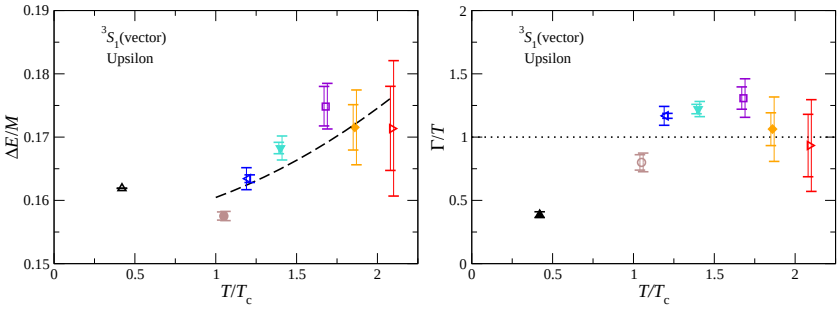

Figure 4. Position of the ground state peak ΔE, normalised by the heavy quark mass (left), and the upper limit on the width of the ground state peak, normalised by the temperature (right), as a function of T/T_c in the vector (Υ) channel. Similar results have been obtained for the pseudoscalar (η_b) channel [5].

with the interpretation of the correlator study presented above and supports the conclusion that the P wave bound states melt in the QGP.

In order to interpret the remaining structure, we compare it with the spectral function computed on the lattice, in the absence of interactions [5]. In Fig. 3, rightmost panel, we show the free lattice spectral functions, together with the spectral functions above T_c. In that plot we have adjusted the threshold to match our lattice results, and once this is done the lattice spectral function and the free one almost coincide. This lends further support to the conclusion drawn in Ref. [4] from an analysis of the correlators: the system in the P wave channels is approaching a system of noninteracting quarks, and the residual interactions can be described by a shift in the quarkonium energies, which does not affect the shape of spectral functions.

5. Comparison with analytic studies and momentum dependence

In this section we restrict our analysis to the S waves. From the computed spectral functions we can determine the mass (from the peak position) and (an upper bound on) the width of the ground state at each temperature.

In Fig. 4 we show the temperature dependence of the mass shift ΔE, normalised by the heavy quark mass and the temperature dependence of the width, normalised by the temperature.

We now contrast our results with analytic predictions derived assuming a weakly coupled plasma [20, 23–28]. According to Ref. [26], the thermal contribution to the width is given, at leading order in the weak coupling and large mass expansion, by

$$\frac{\Gamma}{T} = \frac{1156}{81}\alpha_s^3 \simeq 14.27\alpha_s^3, \tag{9}$$

i.e. the width increases linearly with the temperature. If we take as an estimate from our results that $\Gamma/T \sim 1$, we find that this corresponds to $\alpha_s \sim 0.4$, which

n	(1,0,0)	(1,1,0)	(1,1,1)	(2,0,0)	(2,1,0)	(2,1,1)	(2,2,0)
$\|\mathbf{p}\|$ (GeV)	0.634	0.900	1.10	1.23	1.38	1.52	1.73
v $[\Upsilon(^3S_1)]$	0.0670	0.0951	0.116	0.130	0.146	0.161	0.183
v $[\eta_b(^1S_0)]$	0.0672	0.0954	0.117	0.130	0.146	0.161	0.183

Table 1. Nonzero momenta [6]. Also indicated are the corresponding velocities $v = |\mathbf{p}|/M_S$ of the ground states in the vector (Υ) and pseudoscalar (η_b) channels, using the ground state masses determined previously [4], $M_\Upsilon = 9.460$ GeV and $M_{\eta_b} = 9.438$ GeV.

is a reasonable result. (It would be of interest to compute α_s directly on our configurations.) In the same spirit the thermal mass shift is given in Ref. [26] by

$$\delta E_{\rm thermal} = \frac{17\pi}{9}\alpha_s \frac{T^2}{M} \simeq 5.93\alpha_s \frac{T^2}{M}. \tag{10}$$

In these simulations we have $T_c \sim 220$ MeV, $M \sim 5$ GeV. Taking these values together with $\alpha_s \sim 0.4$ as determined above, Eq. (10) becomes

$$\frac{\delta E_{\rm thermal}}{M} = 5.93\alpha_s \left(\frac{T_c}{M}\right)^2 \left(\frac{T}{T_c}\right)^2 \sim 0.0046 \left(\frac{T}{T_c}\right)^2. \tag{11}$$

In order to contrast our results with this analytical prediction, we have compared the temperature dependence of the peak positions to the simple expression

$$\frac{\Delta E}{M} = c + 0.0046 \left(\frac{T}{T_c}\right)^2, \tag{12}$$

where c is a free parameter. This is shown by the dashed line in Fig. 4 (left panel). The numerical results and the analytic ones are not inconsistent, within the large errors.

The analysis from effective theories predicts significant momentum effects at large momenta. Moreover current CMS results have been obtained at large momenta. There is therefore both phenomenological and experimental motivation to extend these studies to non-zero momenta [6]. The momenta and velocities that are accessible on the lattice are constrained by the discretization and the spatial lattice spacing. The lattice dispersion relation reads

$$a_s^2 \mathbf{p}^2 = 4 \sum_{i=1}^{3} \sin^2 \frac{p_i}{2}, \qquad p_i = \frac{2\pi n_i}{N_s}, \qquad -\frac{N_s}{2} < n_i \leq \frac{N_s}{2}. \tag{13}$$

To avoid lattice artefacts, only momenta with $n_i < N_s/4$ are used: we consider the combinations (and permutations thereof) given in Table 1. The largest momentum, using $\mathbf{n} = (2,2,0)$, is $|\mathbf{p}| \simeq 1.73$ GeV, corresponding to $v = |\mathbf{p}|/M_S \simeq 0.2$. Therefore, the range of velocities we consider is non-relativistic.

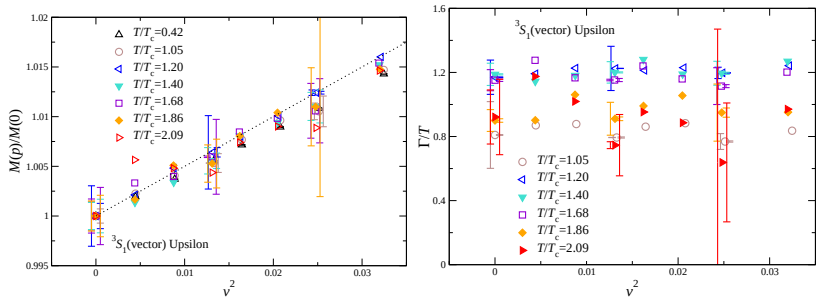

Figure 5. Position of the ground state peak $M(\mathbf{p})/M(0)$ (left) and the upper limit on the width of the ground state peak, normalized by the temperature, Γ/T (right), as a function of the velocity squared (v^2) in the vector (Υ) channel Analogous results have been obtained for the the pseudoscalar (η_b) channel. The dotted line in the left figure represents $M(\mathbf{p})/M(0) = 1 + \frac{1}{2}v^2$ [6].

As in the zero-momentum case, we extract masses and widths from our correlators using MEM, and we display them in Fig. 5. We observe that the peak position increases linearly with v^2, as expected. Assuming the lowest-order, non-relativistic expression $M(\mathbf{p}) = M(0) + \mathbf{p}^2/2M(0)$, one finds

$$\frac{M(\mathbf{p})}{M(0)} = 1 + \frac{\mathbf{p}^2}{2M^2(0)} = 1 + \frac{1}{2}v^2, \tag{14}$$

which is indicated with the dotted lines in the left figures.

The dependence on the velocity can be compared with EFT predictions. In Ref. [28] a study of the velocity dependence was carried out in the context of QED, working in the rest frame of the bound state (i.e. the heat bath is moving). In order to compare with our setup, we consider the case in which the temperature is low enough for bound states to be present and where the velocities are non-relativistic. In that case, one finds [28], in the rest frame of the bound state and at leading order in the EFT expansion,

$$\frac{\Gamma_v}{\Gamma_0} = \frac{\sqrt{1-v^2}}{2v} \log\left(\frac{1+v}{1-v}\right), \tag{15}$$

where Γ_0 is the width at rest. Interpreting the width as an inverse lifetime, one can express this result in the rest frame of the heat bath by dividing with the Lorentz factor $\gamma = 1/\sqrt{1-v^2}$. An expansion for non-relativistic velocities then yields

$$\frac{\Gamma_v}{\Gamma_0} = 1 - \frac{2v^2}{3} + \mathcal{O}\left(v^4\right). \tag{16}$$

If we apply this result to our study of bottomonium, we find that the effect of the nonzero velocity shows up as a correction at the percent level (recall that $v^2 \lesssim 0.04$), which is beyond our level of precision but consistent with the observed v independence within errors. Similarly, additional thermal effects in

the dispersion relation are currently beyond our level of precision. In summary, the observations in our low-momentum range are consistent with Ref. [28], and in order to observe the predicted non-trivial momentum dependence we need to explore larger momenta.

6. From lattice to experiments

We have presented our results for bottomonium in the quark-gluon plasma, for temperatures up to $2.1T_c$, at the threshold of the region currently explored by LHC heavy-ion experiments. Our analysis uses full relativistic dynamics for the light quarks, and a non-relativistic approach for the bottom quarks. The results are amenable to a successful comparison with effective models which we hope to further pursue in the future.

Our results demonstrate a pattern of suppression of bottomonia which apparently compares well with recent CMS results [11, 12], once we take into account that the temperatures reached in the collisions studied by CMS are similar to the ones of our lattices. However the systems under investigation are vastly different: Quantum Chromodynamics in thermal equilibrium in one case, and an expanding fireball, with an extremely complex experimental setup, in the other. For instance, our studies include processes between a b quark and thermal light quarks (and gluons), but do not include the thermal scattering of b quarks. Unravelling the details and the limitations of this comparison is a subject of active research, certainly beyond the scope of this note.

Acknowledgments

We thank Don Sinclair and Bugra Oktay for collaboration. This work was partly supported by the European Community under the FP7 programme HadronPhysics3. We acknowledge the support and infrastructure provided by the Trinity Centre for High Performance Computing and the IITAC project funded by the HEA under the Program for Research in Third Level Institutes (PRTLI) co-funded by the Irish Government and the European Union. The work of CA and GA is carried out as part of the UKQCD collaboration and the STFC funded DiRAC Facility. GA and CA are supported by STFC. GA is supported by the Royal Society, the Wolfson Foundation and the Leverhulme Trust. SK is grateful to STFC for a Visiting Researcher Grant and supported by the National Research Foundation of Korea grant funded by the Korea government (MEST) No. 2012R1A1A2A04668255. SR is supported by the Research Executive Agency (REA) of the European Union under Grant Agreement number PITN-GA-2009-238353 (ITN STRONGnet) and the Science Foundation Ireland, grant no. 11-RFP.1-PHY-3201.

References

[1] Borsanyi S *et al.* [Wuppertal-Budapest Collaboration] 2010 Is there still any T_c mystery in lattice QCD? Results with physical masses in the continuum limit III JHEP **1009** 073

[2] Bazavov A *et al.* [HotQCD Collaboration] 2012 The chiral and deconfinement aspects of the QCD transition Phys. Rev. D **85** 054503

[3] Becattini F 2014 this Volume

[4] Aarts G, Kim S, Lombardo M P, Oktay M S, Ryan S M, Sinclair D K and Skullerud J I 2011 Bottomonium above deconfinement in lattice nonrelativistic QCD Phys. Rev. Lett. **106** 061602
[5] Aarts G, Allton C, Kim S, Lombardo M P, Oktay M B, Ryan S M, Sinclair D K and Skullerud J I 2011 What happens to the Upsilon and η_b in the quark-gluon plasma? Bottomonium spectral functions from lattice QCD JHEP **1111** 103
[6] Aarts G, Allton C, Kim S, Lombardo M P, Oktay M B, Ryan S M, Sinclair D K and Skullerud J I 2013 S wave bottomonium states moving in a quark-gluon plasma from lattice NRQCD JHEP **1303** 084
[7] Aarts G, Allton C, Kim S, Lombardo M P, Ryan S M and Skullerud J I 2013 Melting of P wave bottomonium states in the quark-gluon plasma from lattice NRQCD JHEP **1312** 064
[8] Aarts G, Allton C, Kelly A, Skullerud J I, Kim S, Harris T, Ryan S M, Lombardo M P *et al.* 2013 Bottomonium from lattice QCD as a probe of the Quark-Gluon Plasma J. Phys. Conf. Ser. **432** 012014
[9] Allton C, Aarts G, Amato A, Evans W, Giudice P, Hands S, Kelly A, Kim S *et al.* 2013 Quark-Gluon Plasma phenomenology from the lattice (*Preprint* arXiv:1310.5135)
[10] Rapp R and van Hees H 2010 Heavy Quarks in the Quark-Gluon Plasma *R. C. Hwa, X.-N. Wang (Ed.) Quark Gluon Plasma 4, World Scientific, 111*
[11] Chatrchyan S *et al.* [CMS Collaboration] 2011 Indications of suppression of excited Υ states in PbPb collisions at $\sqrt{S_{NN}} = 2.76$ TeV Phys. Rev. Lett. **107** 052302
[12] Chatrchyan S *et al.* [CMS Collaboration] 2012 Observation of sequential Upsilon suppression in PbPb collisions Phys. Rev. Lett. **109** 222301
[13] Morrin R, Ó Cais A, Peardon M, Ryan S M and Skullerud J I 2006 Dynamical QCD simulations on anisotropic lattices Phys. Rev. D **74** 014505
[14] Oktay M B and Skullerud J I 2010 Momentum-dependence of charmonium spectral functions from lattice QCD (*Preprint* arXiv:1005.1209)
[15] Aarts G, Allton C, Harris T, Kim S, Lombardo M P, Ryan S M and Skullerud J I 2014 The bottomonium spectrum at finite temperature from $N_f = 2 + 1$ lattice QCD (*Preprint* arXiv:1402.6210)
[16] Burnier Y, Laine M and Vepsalainen M 2008 Heavy quarkonium in any channel in resummed hot QCD JHEP **0801** 043.
[17] Orlandini G 2014 this Volume.
[18] Asakawa M, Hatsuda T and Nakahara Y 2001 Maximum entropy analysis of the spectral functions in lattice QCD Prog. Part. Nucl. Phys. **46** 459
[19] Rothkopf A 2013 Improved Maximum Entropy Analysis with an Extended Search Space J. Comput. Phys. **238** 106
[20] Burnier Y and Rothkopf A 2013 A novel Bayesian approach to spectral function reconstruction Phys. Rev. Lett. **111** 182003
[21] Kim S, Petreczky P and Rothkopf A 2013 Lattice NRQCD study of in-medium bottomonium states PoS LATTICE **2013** 169
[22] Harris T, Ryan S M, Aarts G, Allton C, Kim S, Lombardo M P and Skullerud J I 2013 Bottomonium spectrum at finite temperature (*Preprint* arXiv:1311.3208)
[23] Laine M, Philipsen O, Romatschke P and Tassler M 2007 Real-time static potential in hot QCD JHEP **0703** 054
[24] Laine M 2007 A Resummed perturbative estimate for the quarkonium spectral function in hot QCD JHEP **0705** 028
[25] Brambilla N, Ghiglieri J, Vairo A and Petreczky P 2008 Static quark-antiquark pairs at finite temperature Phys. Rev. D **78** 014017
[26] Brambilla N, Escobedo M A, Ghiglieri J, Soto J and Vairo A 2010 Heavy Quarkonium in a weakly-coupled quark-gluon plasma JHEP **1009** 038
[27] Brambilla N, Escobedo M A, Ghiglieri J and Vairo A 2011 Thermal width and gluodissociation of quarkonium in pNRQCD JHEP **1112** 116
[28] Escobedo M A, Soto J and Mannarelli M 2011 Non-relativistic bound states in a moving thermal bath Phys. Rev. D **84** 016008